

Motion, Creation and Annihilation of Disclinations in Multi-Domain Structured Nematic Liquid Crystal Cells

M. Reichenstein*, H. Stark[‡], J. Stelzer[†], and H.-R. Trebin*

**Institut für Theoretische und Angewandte Physik, Universität Stuttgart,
Pfaffenwaldring 57, D-70550 Stuttgart, Germany*

[‡]*Fachbereich Physik, Universität Konstanz, 78457 Konstanz, Germany*

[†]*Schwetzingen Str. 20, 69190 Walldorf (Baden), Germany*

We study dynamical processes in a multi-domain (MD) structured nematic liquid crystal cell with a particular emphasis on the motion, creation and annihilation of disclinations. In the MD cell right- and left-handed director helices alternate due to a special choice of the director pretilt angles at the surfaces. As a result, a net of twist disclinations occurs. We have implemented a numerical algorithm based on a pure rotational dynamics of the director field to monitor the motion of the defect lines during the switching process, *i.e.*, when an electric voltage is applied to or removed from the cell. We demonstrate that the total light transmission versus time is not affected by the presence of the defects compared to a conventional twisted nematic (TN) cell. If the pretilt angles at the surfaces are sufficiently small, the twisting sense of one species of helices is reversed and a configuration free of defects occurs. On the other hand, for an applied voltage twist disclinations close to the surface have to exist. Therefore, defect lines are created or they annihilate during the switching process. We investigate these situations in detail and reveal the underlying mechanisms.

I. INTRODUCTION

Liquid crystal displays (LCDs) take a very important position in modern information technology (IT). They are economical both in their consumption of energy and their request of space. Recent developments including optical compensation and in-plane switching (IPS) [1] technology improve the quality of high-end LCDs applied in monitors. While these techniques are too expensive for the production of cheap, low-end displays, simpler solutions for one of the main problems are required: the contrast of conventional displays based on the twisted nematic (TN) cell [2] strongly depends on the viewing angle. The multidomain cell (see [3,4] and references cited in these articles) is a very simple approach to reduce this deficiency.

In the classical TN cell the liquid crystal molecules at the two confining glass plates are anchored parallel to the surface. They enclose an angle of 90° so that the molecules in the bulk form a helix. By slightly tilting the molecules at the surface, the twisting sense of the helix can unambiguously be chosen left or right. In the standard TN cell, the molecules in the bulk are always

completely aligned along the electric field by applying a sufficiently high voltage. In a TN greyscale display, different grey values are achieved by varying the applied voltage. The molecules are not fully aligned along the electric field. Their direction is governed by an equilibrium between elastic and electric torques. The helical structure is still partly recognizable. Since all the helices have the same twisting sense, the inversion symmetry of the TN cell is broken. As a result the contrast strongly depends on the viewing angle.

The basic idea of the multi-domain (MD) concept is to avoid this symmetry breaking. The two surfaces of the cell are treated such that alternating domains of left- and right-handed helices occur like on a chessboard (see Fig. 1). The optical effects of the different domains compensate each other at the length scale of the display pixel, and hence the dependence of the contrast on the viewing angle is strongly reduced. Different surface treatments are employed to realize the MD concept [5,3,4,6]. The improvement in the contrast is clearly visible.

Since helices of different twisting sense do not match, all realizations of the MD cell exhibit a characteristic net of line defects situated at the border of the domains. The radial extension of the disclination core is of the order of 10 nm, *i.e.*, much smaller than the width of one domain which amounts to $100 \mu\text{m}$. Therefore, the disclinations can be neglected for the contrast properties of the display.

However the occurrence of the disclination lines depends on the choice of the tilt angle of the molecules at the surface. The free energy of a disclination line consists of a core and an elastic part. By reversing the twisting sense of one species of helices, the disclinations are eliminated.

To accommodate the helices with the unfavorable twisting sense, additional splay deformations close to the surfaces have to be introduced. If their elastic free energy is less than the core energy of the disclination lines, the defect free configuration occurs. The reverse phenomena, the avoidance of splay deformations by introducing alternative distortions or even disclinations as in the case of the MD cell, is denoted *splay canceling* [7,8,4]. It appears for surface tilt angles θ_p smaller than a maximum value θ_p^D , as illustrated in the configuration phase diagram of Fig. 2. Note that we measure the tilt angle with respect to the normal of the plates. Then $\theta_p = 90^\circ$ means that the molecules are parallel to the surface. The figure is reproduced from Ref. [9] where we investigated splay

cancelling by numerical means.

When the MD technique is used in displays, the surface anchoring has to be chosen in such a way that the chessboard pattern of left- and right-handed helices and therefore the disclination lines are always present, particularly at zero voltage. This corresponds to the lower path in Fig. 2. In section III A we will discuss the switching process of such a cell.

From a theoretical point of view the upper path in Fig. 2 is of greater interest. The configuration at $U = 0$ V consists of helices with a common twisting sense whereas the director field in area I contains disclination lines. Therefore, during the switching process a configurational transition must take place where disclinations are created or disappear. In section III B, we examine the switching process along the upper dotted line. We investigate in detail how disclinations are nucleated via ring defects and how they are removed when line defects cross each other.

The paper is organized as follows. In Section II we introduce the geometry of our problem, summarize the theory, and introduce the numerical methods to investigate the dynamical properties of the MD cell. In addition, we provide an automated search for disclinations and explain the visualization of the transmitted light. In Section III the results of the simulations are presented, and we finish with conclusions in Section IV.

II. GEOMETRY, THEORY AND NUMERICAL ALGORITHMS

A. Geometry

In our simulations we use a realization of the multi-domain cell introduced by Schadt *et al.* [3]. Figure 1 gives a schematic view of the cell. Cartesian coordinates are used to describe the cell geometry. The average direction of the molecules is characterized by the director \mathbf{n} . Since it is a unit vector, we employ a twist (ϕ) and tilt (θ) angle to parametrize its Cartesian components: $n_x = \sin\theta \cos\phi$, $n_y = \sin\theta \sin\phi$, and $n_z = \cos\theta$. Due to a special surface treatment the lower and upper glass plates are divided into stripes pointing along the x or y axis, respectively.

At both plates the surface tilt angle θ_p assumes a common value during a simulation run, while the surface twist angle ϕ_p varies for each stripe according to Table I. The result of such a surface anchoring structure are domains of director helices with alternating twisting sense. Since helices of opposite twisting sense do not match, a net of crossed twist disclinations should occur.

The unit cell of our simulation box has a width and depth of $2b$, and its thickness is d . We employ periodic boundary conditions along the x and y direction. To avoid disclinations at the boundary of the simulation box, we shifted the unit cell by $b/2$ along the x and y direction compared to Fig. 1. The final simulation box is

illustrated in Fig. 3. For the lengths we chose $b = 9\mu\text{m}$ and $d = 6\mu\text{m}$.

B. Equations and their Numerical Solution

To obtain an initial configuration for our dynamic simulations, we first minimize the total free energy F of the simulation box. It consists of two parts: the elastic or Frank free energy and the electric free energy:

$$F = \int [f_{\text{elast}}(\mathbf{x}) + f_{\text{elec}}(\mathbf{x})] d^3x . \quad (1)$$

The Frank free energy density $f_{\text{elast}}(\mathbf{x})$ describes elastic distortions in the director field $\mathbf{n}(\mathbf{x})$. It can be divided into three basic modes with their corresponding elastic constants splay (k_{11}), twist (k_{22}) and bend (k_{33}):

$$f_{\text{elast}}(\mathbf{x}) = \frac{1}{2}k_{11}(\text{div } \mathbf{n})^2 + \frac{1}{2}k_{22}(\mathbf{n} \cdot \text{curl } \mathbf{n})^2 + \frac{1}{2}k_{33}(\mathbf{n} \times \text{curl } \mathbf{n})^2 . \quad (2)$$

In the nematic phase \mathbf{n} and $-\mathbf{n}$ describe the same situation. This symmetry enables, *e.g.*, the existence of disclination lines. In a numerical simulation, one has to discretize the director derivatives. In order to avoid artificial derivatives which occur when neighboring directors are nearly anti-parallel to each other, they always have to be aligned along each other. To surpass this difficulty, we rewrite the free energy with the help of the symmetric and traceless order parameter field $\mathbf{Q}(\mathbf{x})$ of second rank. In the uniaxial nematic phase its Cartesian components are

$$Q_{ij} = n_i n_j - \frac{1}{3}\delta_{ij}, \quad i, j = 1, 2, 3, \quad (3)$$

where n_i is the i -th component of the director and δ_{ij} is the Kronecker symbol. We do not introduce the Maier-Saupe order parameter S since it is constant in the nematic phase. With the help of scalar invariants of Q_{ij} and $Q_{ij,k}$ (k denotes a spatial derivative along the x_k axis), the Frank free density can be written in terms of Q_{ij} and $Q_{ij,k}$ [10]:

$$f_{\text{elast}}(\mathbf{x}) = \frac{1}{12}(3k_{22} - k_{11} + k_{33})Q_{ij,k}Q_{ij,k} + \frac{1}{2}k_{11}Q_{jk,k}Q_{jl,l} - \frac{1}{2}k_{22}Q_{jk,l}Q_{jl,k} + \frac{1}{4}(k_{33} - k_{11})Q_{jk}Q_{lm,j}Q_{lm,k} \quad (4)$$

Substituting Eq. (3) into Eq. (4), the Frank free energy density (2) is recovered.

The voltage applied to the plates of the MD cell induces an electric field. Its electric free energy in terms of the electric potential U is

$$f_{\text{elec}}(\mathbf{x}) = \frac{1}{2} \epsilon_0 \Delta \epsilon \left(\frac{\epsilon_{\parallel} + 2\epsilon_{\perp}}{3(\epsilon_{\parallel} - \epsilon_{\perp})} \delta_{ij} + Q_{ij} \right) U_{,i} U_{,j}, \quad (5)$$

where ϵ_{\parallel} and ϵ_{\perp} are the eigenvalues of the dielectric tensor $\epsilon_{ij} = \epsilon_{\perp} \delta_{ij} + (\epsilon_{\parallel} - \epsilon_{\perp}) n_i n_j$. They stand for the dielectric constants parallel and perpendicular to the director. The dielectric anisotropy is $\Delta \epsilon = \epsilon_{\parallel} - \epsilon_{\perp}$.

The minimum of the free energy F is found by solving the Euler-Lagrange equations for the three independent scalar fields, *i.e.*, the tilt angle $\theta(\mathbf{x})$, the twist angle $\phi(\mathbf{x})$, and the electric potential $U(\mathbf{x})$. With the help of the following chain rule for functional derivatives [11], we can employ the Frank free energy density f_{elast} in the \mathbf{Q} representation (see Eq. 4) to set up the Euler-Lagrange equations:

$$\begin{aligned} \frac{\delta F}{\delta w} &= \frac{\delta F}{\delta Q_{ij}} \frac{\delta Q_{ij}}{\delta w} \\ &= \left[\frac{\partial f}{\partial Q_{ij}} - \frac{\partial}{\partial x_m} \frac{\partial f}{\partial (Q_{ij,m})} \right] \frac{\delta Q_{ij}}{\delta w} = 0 \end{aligned} \quad (6)$$

where w stands for ϕ or θ . Einstein's summation convention is used. The Euler-Lagrange equation for U is

$$\frac{\delta F}{\delta U} = \frac{\partial f}{\partial U} - \frac{\partial}{\partial x_m} \frac{\partial f}{\partial (U_{,m})} = 0. \quad (7)$$

The Euler-Lagrange equations were discretized on a Cartesian lattice and a standard Newton-Gauß-Seidel procedure was employed [12] to solve them. The calculated minimum energy configurations then served as initial configurations for the dynamic simulations.

To handle the dynamics of a MD cell, we employed a pure rotational dynamics of the director field without any coupling to the velocity field [13]:

$$\frac{\delta F}{\delta \theta} = -\gamma \frac{\partial \theta}{\partial t}, \quad \frac{\delta F}{\delta \phi} = -\gamma \frac{\partial \phi}{\partial t} \sin^2 \theta, \quad (8)$$

where γ is a typical rotational viscosity. They were solved by an explicit time integration method [12]. The electric potential U was assumed to adjust instantaneously to the director rotation time scale, so that the static equation (7) was solved at each time step.

Throughout all the simulations the values for the material parameters were chosen as in [14]: $k_{11} = 12.4 \cdot 10^{-12}$ N, $k_{22} = 6.5 \cdot 10^{-12}$ N, $k_{33} = 19.9 \cdot 10^{-12}$ N, $\epsilon_{\parallel} = 8.03$, $\epsilon_{\perp} = 3.59$, and $\gamma_1 = 17 \cdot 10^{-3}$ Nsm⁻².

At last we add a note about the disclinations. In our simulation we did not introduce an extra core energy for reasons of simplicity. As the length of the disclinations varies, it would have been too complicated numerically to correct for the core energy at each time step.

C. Automated Search for Defects and Visualization

We developed some tools to visualize the director field configuration in the MD cell. Especially, we have implemented an algorithm of automated Burgers circuits to

detect disclinations automatically. The algorithm adopts the conventional definition of a line defect to a grid of lattice points. To detect a line defect at a certain lattice point, we move around it on a loop of nearest neighbours. When moving from one lattice point to the next, the directors are aligned such that they enclose an angle smaller than 90°. At last, we compare the directors at the starting and end point of the loop. If they enclose an angle larger than 90°, a line defect is present. Whenever the angle between two neighboring directors on a loop is very close to 90°, the search is performed on a loop of next-nearest neighbors. To obtain a three-dimensional picture of the position of the disclination lines, we use the Virtual Reality Modeling Language [15]. Each defect position on the grid is marked by a small sphere. All spheres together present an image of the disclination line.

We also calculated the optical transmission for light incident parallel to the surface normal of the plates (*i.e.*, along the negative z axis) based on the 2×2 Jones-matrix method [16]. The incident light is polarized along the x axis at $z = d$, and it is analysed by a polarizer along the y axis at $z = 0$ after being modified by the liquid crystal. The resulting intensity is mapped onto a greyscale. Maximum transmission corresponds to white and minimum transmission to black. The resulting grey values for each grid point in the xy plane represent the transmission pattern of the liquid crystal configuration. In our calculations we always used monochromatic light of wavelength $\lambda = 544$ nm. The refractive indices were $n_{\perp} = 1.489$ and $n_{\parallel} = 1.762$.

III. SWITCHING THE MD CELL

In this section we investigate the dynamic processes in the MD cell which take place during a switching process, *i.e.*, after an electric voltage of 4 V has been applied to or removed from the cell. We first comment on the configuration as it is used in displays, where the net of disclinations is always present (subsection III A). Then we consider the upper switching path in the phase diagram of Fig. 2. A configurational transition occurs where line defects have to be created or removed from the cell (subsection III B).

All the simulations presented were performed on a grid with 40 gridpoints in x , y and z direction, respectively. All switching times referred to in the following text and the figures are measured in milli seconds.

A. The MD Cell as a Display

It would be natural to study the switching process along the lower path in Fig. 2. However, we note that the tilt angle $\theta_p^D = 58^\circ$ below which the disclinations are always present is much smaller compared to realizations

of the MD display. For example, Schadt *et al.* work at a tilt angle of $\theta_p = 88.7^\circ$ [3]. Chen *et al.* have studied the occurrence of splay canceling in the MD cell in detail [17], and they even fabricated a display with θ_p^D as small as 65° . With a rough estimate, the authors could show that the value of θ_p^D depends on the ratio of cell dimensions.

If the director helix is reversed, an additional splay distortion is distributed over the whole subpixel. Its total energy for two subpixels is approximated as an average Frank free energy density times the volume $2b^2d$, *i.e.*,

$$F_S \simeq K \left(\frac{2(\pi/2 - \theta_p)}{d} \right)^2 b^2d . \quad (9)$$

The twist disclinations occur if their core energy F_d is smaller than F_S . The core energy is given by

$$F_d = 8Kb , \quad (10)$$

where the average Frank constant K approximates the line energy of a defect core. The transition between both configurations takes place at $F_S \approx F_d$ or

$$\theta_p^D \approx \pi/2 - \sqrt{2d/b} . \quad (11)$$

With the parameters of our numerical calculations, $d/b = 1/3$, we find $\theta_p^D = 43^\circ$ which deviates from the simulated value, $\theta_p^D = 58^\circ$, due to the rough estimates for the free energies involved. However, Eq. (11) demonstrates that the relatively small angle of 58° results from the small lateral extension $b = 18\mu\text{m}$ compared to typical pixel sizes of $100\mu\text{m}$.

To be closer to the experimental realization of the MD display, we decided to study the switching process for a cell with pretilt angle $\theta_p = 85^\circ$. At zero voltage ($U = 0\text{V}$) the defect configuration can nevertheless be prepared since it corresponds to a metastable state. We construct it by solving the static equation (6). Then we set the voltage to 4V and start the time integration algorithm. For characteristic times in the evolution of the director field, we plot in Fig. 4 the disclination lines in the cell and in the lower right corner its light transmission.

At $t = 0$, the defect lines are situated in the center of the cell forming a net of twist disclinations. When the voltage is turned on, the disclinations start to move towards the glass plates (see Fig. 4, $t = 0.84$ and 1.20). At their intersections they are dipped towards each other, due to an attractive interaction. When they have reached the bounding surfaces, they straighten out (see Fig. 4, $t = 1.80$). It is instructive to consider the light transmission. At $t = 0$, the disclinations can hardly be seen in the transmission pattern. When they move towards the glass plates, the contrast becomes stronger, *i.e.*, close to the disclinations the cell switches faster compared to the rest of the display. This surprising result is also illustrated in Fig. 5 where we plot the transmission versus time close to the defect lines (curve b) and in the center of the display

(curve a). The dip in curve a between $t = 0.5$ and 1 is a well known phenomenon in a TN cell with pretilt [18]. The transmission characteristic of a TN cell (see curve c) is also plotted in Fig. 5. It demonstrates that far away from the disclination lines the helices in the MD cell switch nearly as fast as in a pure TN display. Since the lateral extension of a pixel is much larger than the core of a twist disclination, we can conclude that the motion of the defect lines does not influence the light transmission of a MD display.

We finish with two remarks. First, when the voltage is turned off, the motion of the disclination lines, as illustrated in the snapshots of Fig. 4, is simply reversed.

Secondly, the position of the twist disclinations as a function of the pretilt angle θ_p for zero voltage is the following. Until $\theta_p = 80^\circ$ the defect lines are straight and located in the center of the cell. Below $\theta_p = 80^\circ$ they start to bend moving towards the glass plates but still touching each other at the intersections. At $\theta_p = 60^\circ$, the lines lose contact, and for further decreasing θ_p they move closer to the surface.

B. Configurational Transitions in the MD Cell

1. Switching from 0V to 4V

For the upper path in Fig. 2, we calculate the initial configuration by solving the static equation (6) for 0V . As before, the voltage is set to 4V , and the time integration algorithm is started. Snapshots of the appearing disclination lines and the light transmission patterns are illustrated in Fig. 6.

At $t = 0.0$ all helices have a common twisting sense. The helices of the RHDs (see Fig. 3) turn in accordance with their boundary conditions. The helices in the LHDs have reversed their twisting sense by introducing an additional splay deformation which is distributed over the whole helix. No disclinations are present. Now the voltage of 4V is applied and the directors start to align along the electric field. At $t = 3.6$ a clear difference can be seen between the two types of helices: In the RHDs the transmission is already close to zero, *i.e.*, the helix is destroyed since the directors are parallel to the electric field. In the LHDs the transmission is almost unchanged. The helix structure is still present. We understand that feature from Fig. 7(a) where we present a schematic nail picture of the helices along a path indicated in the snapshots of the cell in Fig. 6. Note that the length of the nail is given by the projection of the director on the drawing plane and that the head symbolizes the part of the director below the drawing plane.

In the first and second helix all directors are commonly tilted towards the electric field, and they can align along the field immediately. However, the third and fourth helix, whose twisting sense is reversed by an additional

splay deformation, are temporarily stabilized by the occurrence of a horizontal director. At $t = 14.88$, also the directors in the LHDs are aligned along the electric field [see fourth helix in Fig. 7(b)] leaving two bright stripes in the transmission pattern. They result from regions symbolized by the second and third helix in Fig. 7(b) whose directors can only be aligned along the electric field by introducing a $+\frac{1}{2}$ wedge (W) and a twist (T) disclination, as illustrated in Fig. 7(c). These disclinations are part of one of the two defect rings which start to open up in the xz plane at $t = 14.88$ and then grow continuously. Upon touching each other at $t = 17.66$, they annihilate leaving a wedge and a twist disclination at the upper and lower plate, respectively. The line defects straighten out until $t = 32.35$. Note that due to the creation of the two defect lines, one bright stripe has vanished in the transmission pattern.

At $t = 32.35$ the simulation is trapped in a local minimum. To reach the global minimum a second pair of disclinations should have been created to reduce the transmission of the second white stripe. But even then the cell is not in its global minimum configuration since the disclination lines at the upper plate have to point along the y axis. To achieve a rotation of the defect lines, we propose the following mechanism. In Fig. 8(I) the defect lines at the upper plates are drawn. Note that in the regions 1 to 4 an additional splay deformation close to the upper surface is still present. An inspection of the director field reveals that this splay deformation can be reduced locally by opening up a disclination rings [see Fig. 8(I)]. Their right and left parts are twist disclinations whereas the upper and lower parts have a wedge character. The latter ones annihilate with the existing wedge disclinations [see Fig. 8(II)], and the twist parts of the disclination ring produce the two required defect lines parallel to the y axis.

The final director field of the global minimum consists of two pairs of disclinations, parallel to the surface anchoring stripes of the respective glass plates. It is taken as initial configuration in the following section as illustrated in Fig. 9, $t = 0.0$.

2. Switching from 4V to 0V

In Fig. 9 we illustrate the evolution of the MD cell after the voltage of 4V has been removed at $t = 0.0$. The disclination pattern and the transmission of light are shown. At $t = 0.0$ the directors are still aligned along the z axis parallel to the electric field direction. The helices are destroyed and the intensity of the transmitted light is zero. The twist disclinations are located close to the surfaces. When the voltage is removed, the director field relaxes due to the elastic interactions. At $t = 2.42$ the helices in the LHDs and RHDs are restored.

The director configuration has regained its ability to rotate the polarization of light, and the transmission is

almost at its maximum. Fig. 9, $t = 2.42$, reveals that the disclinations have moved towards the center of the cell. They are clearly visible in the transmission. At $t = 5.36$ the disclinations start to dip towards each other due to a strong attraction in the region of their crossing sections. Then, at $t = 6.77$, recombinations of the disclinations take place which are completed at $t = 12.12$ when a net of disclinations is situated at the center of the cell at $z = d/2$.

So far, the situation is similar to the MD display discussed in subsection III A. Here, the intersections of the disclinations eventually break up such that two line defects result (see Fig. 9, $t = 17.64$) which straighten out until $t = 42.00$. They separate domains with right- and left-handed helices. Now, our simulation is trapped in a local minimum, and the configuration does not change any more. The global minimum would be helices with a common twisting sense. It can be reached by the following scenario. At $t = 12.12$ the intersections of the line defects should break up such that a ring disclination in the center of the cell occurs which shrinks and ultimately annihilates leaving a defect-free configuration. Whether this scenario does not appear in our simulation due to numerical inaccuracies or whether it is very unlikely to happen since the intersections have to break up in a very defined way, has to be answered by an experimental investigation.

IV. CONCLUSIONS

The concept for the MD cell emerged from the need to improve the viewing angle of the conventional liquid crystal display based on the TN cell. In this paper we have studied one realization of the MD cell in detail. By tilting the director against the planar orientation at the surface, a chessboard pattern of alternating left- and right-handed helices is expected where topology requires the existence of twist disclinations. For sufficiently small tilt angles θ_p against the surface normal, the pattern exists. However, if θ_p is increased, the twisting sense of one species of helices is reversed at the cost of an additional splay deformation. Following Chen *et al.* [17], we have given an estimate for the tilt angle θ_p^D where a transition between both configurations occurs. It solely depends on the ratio of the cell dimensions.

We have implemented a numerical algorithm based on a pure rotational dynamics of the director field to study the dynamics of the MD cell which is driven by an electric field. Furthermore, we have developed tools to visualize the defect dynamics and the transmission of light. In the realization of the display, where the line defects are always present, we find that the total transmission versus time is not affected compared to a conventional TN cell. Although, as a surprising result, the switching time close to the disclinations is smaller. From a theoretical point of view, the second configuration without defects at zero

voltage is more appealing. It provides a playground for studying the creation and annihilation of line defects. We have investigated these processes for the MD cell in detail, and we have revealed their mechanisms. E.g., when the voltage is turned on, defect rings with a mixed twist and wedge character are nucleated. They partly annihilate to create two twist disclinations at the surface. An obstacle of our simulations is that the dynamics becomes trapped in a metastable minimum and does not relax into the global minimum. Therefore, to check our results, an experimental investigation would be helpful.

M. R. gratefully acknowledges a grant from the Sonderforschungsbereich 382 of the Deutsche Forschungsgemeinschaft. H. S. is generously supported by the Deutsche Forschungsgemeinschaft through a Heisenberg scholarship.

-
- [1] M. Oh-e and K. Kondo. Appl. Phys. Lett. **67** 3895 (1995).
 - [2] M. Schadt and W. Helfrich. Appl. Phys. Lett. **18**, 127 (1971).
 - [3] M. Schadt, H. Seiberle, and A. Schuster. Nature **318**, 212 (1996).
 - [4] J. Chen, P. J. Bos, D. L. Johnson, *et al.*. Jpn. J. Appl. Phys. **35**, 558 (1996).
 - [5] J. Chen, P. J. Bos, D. R. Bryant, D. L. Johnson, *et al.*. Appl. Phys. Lett. **67**, 1990 (1995).
 - [6] J. Li, E. S. Lee, H. Vithana, and P. J. Bos. Jpn. J. Appl. Phys. **35**, 1446 (1996).
 - [7] M. J. Press and A. S. Arrott. J. Phys. (Paris) Coll. C1 **36**, 177 (1975).
 - [8] O. D. Lavrentovich and Y. Nastishin. Europhys. Lett. **12**, 135 (1990).
 - [9] M. Reichenstein, T. Seitz, and H.-R. Trebin. Mol. Cryst. Liq. Cryst. **330**, 549 (1999).
 - [10] L. Longa, D. Monselesan, and H. R. Trebin. Liq. Cryst. **2**, 769 (1987).
 - [11] H. Stark. Eur. Phys. J. B **10**, 311 (1999).
 - [12] W. H. Press. *Numerical Recipes in C: The Art of Scientific Computing*. Academic Press, Cambridge, 2nd edition (1992).
 - [13] G. Vertogen and W. H. de Jeu. *Thermotropic Liquid Crystals, Fundamentals*. Springer-Verlag (1988).
 - [14] M. Schadt, K. Schmitt, V. Kozinkov, and V. Chigrinov. Jpn. J. Appl. Phys., Pt. 1 **31**, 2155 (1992).
 - [15] web3D Consortium. <http://www.vrml.org>.
 - [16] P. S. Drzaic. *Liquid Crystal Dispersions*, volume 1 of *Series on Liquid Crystals*. World Scientific Publishing, Singapore (1995).
 - [17] J. Chen, J. Li, D. L. Johnson, and P. J. Bos. Mol. Cryst. Liq. Cryst. **302**, 151 (1997).
 - [18] J. Stelzer, R. Hirning, and H.-R. Trebin. J. Appl. Phys. **74**, 6046 (1993).
-

coordinates	surface twist angle	surface tilt angle	applied voltage
$z = 0, 0 < y < b$	$\phi_p = 0^\circ$	θ_p	$U = 0 \text{ V}$
$z = 0, b < y < 2b$	$\phi_p = 180^\circ$	θ_p	$U = 0 \text{ V}$
$z = d, 0 < x < b$	$\phi_p = 90^\circ$	θ_p	$U = 0 \text{ or } 4 \text{ V}$
$z = d, b < x < 2b$	$\phi_p = 270^\circ$	θ_p	$U = 0 \text{ or } 4 \text{ V}$

TABLE I. Surface anchoring structure for the cell in Fig. 1 and the electric potential U at the surfaces. The quantities θ_p and U are parameters in the simulation.

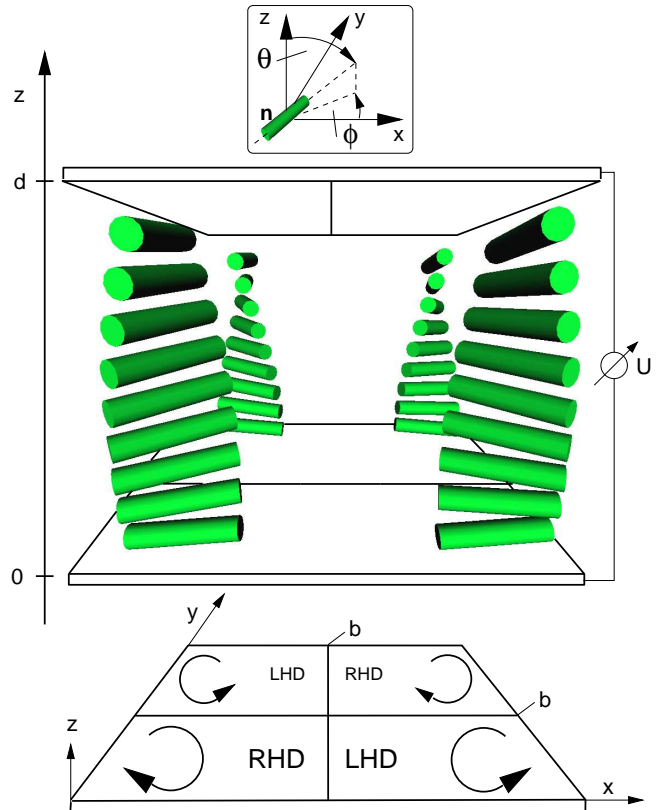


FIG. 1. Schematic view of the multi-domain cell configuration studied in this article: The bottom and top plates are situated at $z = 0$ and $z = d$. They are divided into stripes of width b along the x or the y axis, respectively. The nematic director is described by spherical coordinates ϕ (polar or twist angle) and θ (azimuthal or tilt angle). The anchoring at the plates is such that the director at the surface is aligned along the stripes. Its tilt angle θ_p is fixed, however the twist angle ϕ_p varies by 180° when going from one stripe to the other as summarized in Table I. As a result of such an anchoring structure, a chessboard pattern of domains with left-handed (*LHD*) and right-handed (*RHD*) helices is expected.

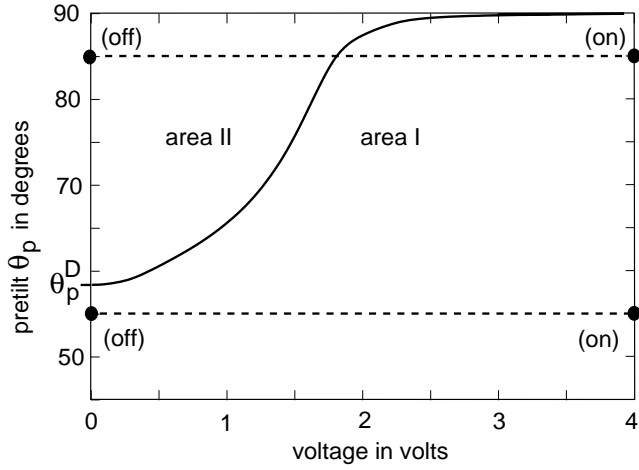


FIG. 2. Configuration phase diagram of the multi-domain cell reproduced from Ref. [9]. Two areas can be distinguished. Area I: Disclination lines are present as expected due to the boundary conditions. Area II: For low voltages and pretilt angles close to planar anchoring, the disclination lines are removed due to the inverse process of splay canceling. All helices possess a common twisting sense. Two switching processes are investigated in the following, one along the upper path at $\theta_p = 85^\circ$ and a second one in analogy to the lower path.

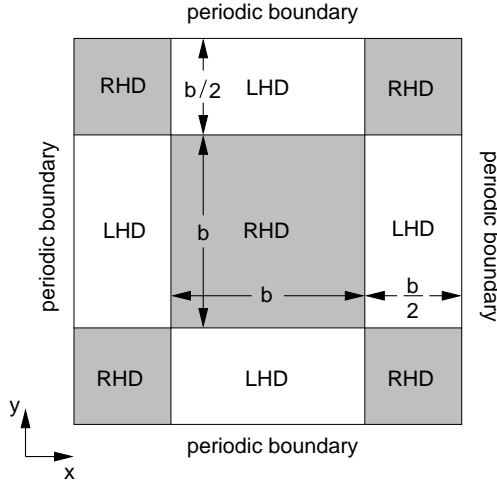


FIG. 3. Simulation box for the MD cell. Compared to Fig. 1, the unit cell is shifted by $b/2$ along the x and y direction to avoid disclination lines at the boundary of the box.

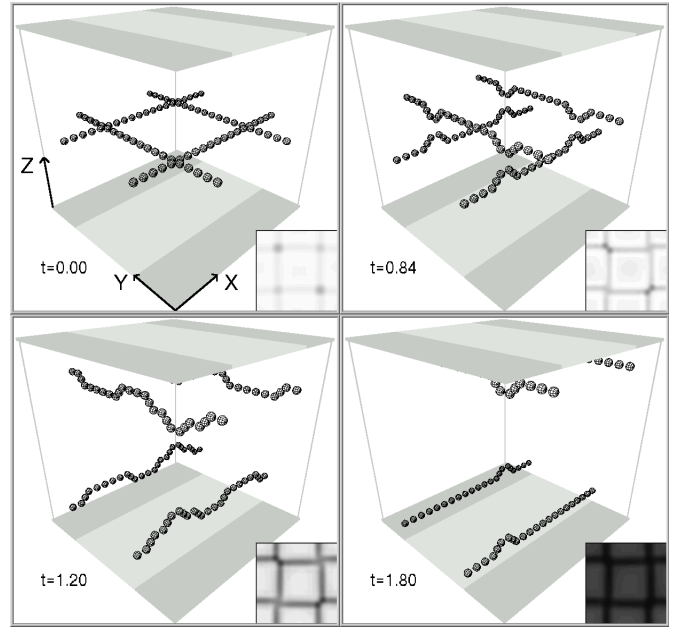


FIG. 4. Snapshots of the moving twist disclinations in the MD display and its transmission of light (see lower right corner) at various time steps after switching the electric voltage from $U = 0$ V to 4 V. The upper and lower glass plates are divided into anchoring stripes shown in dark and light grey. The director field between the two plates is hidden to enlarge the visibility of the disclination lines. For a detailed description refer to the text.

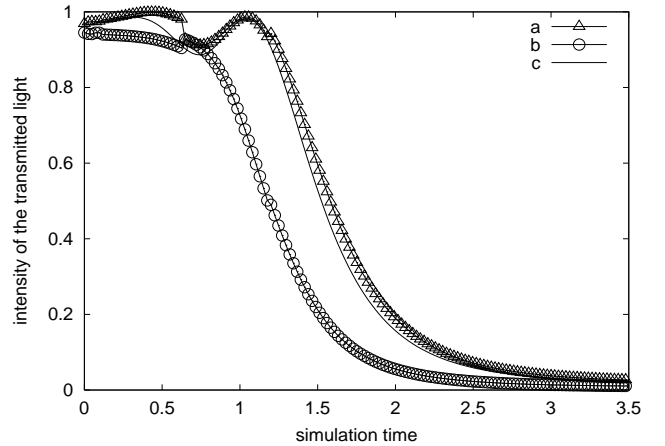


FIG. 5. Light transmission versus time in the MD display: a) in the center of the cell, b) close to a twist disclination, and, for comparison, in the TN cell (curve c).

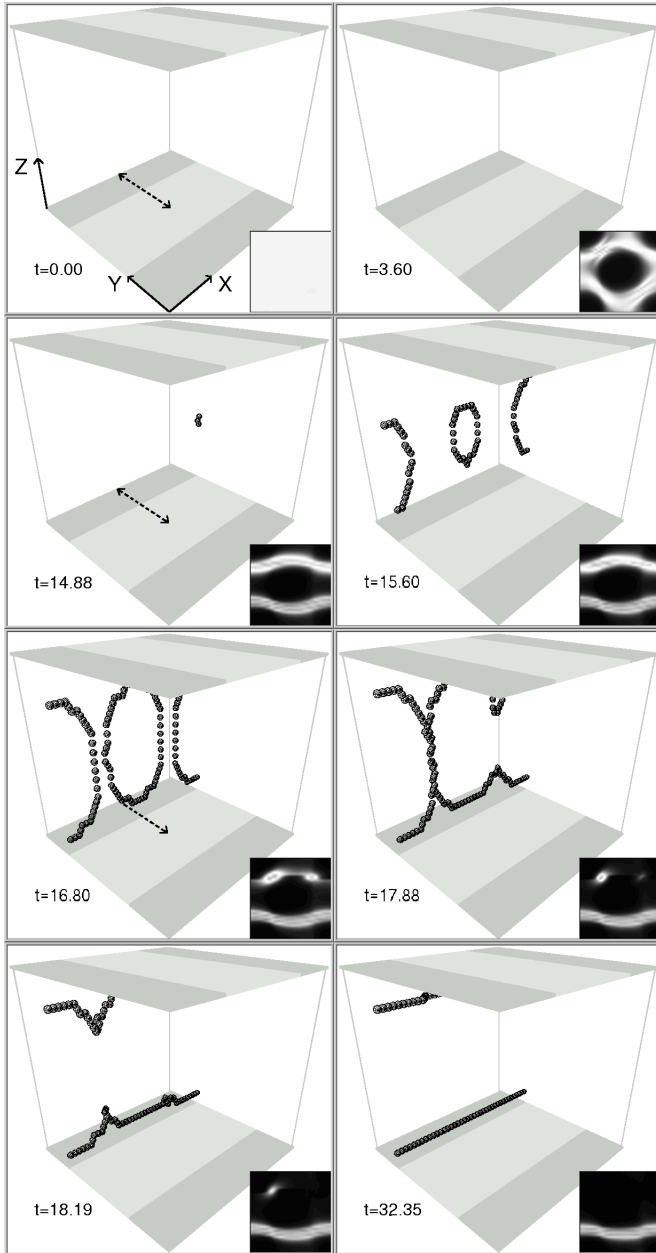


FIG. 6. Snapshots of the creation of disclinations in the MD cell and its transmission of light (see lower right corner) at various time steps after switching the electric voltage from $U = 0$ V to 4 V. The upper and lower glass plates are divided into anchoring stripes shown in dark and light grey. For a detailed description refer to the text.

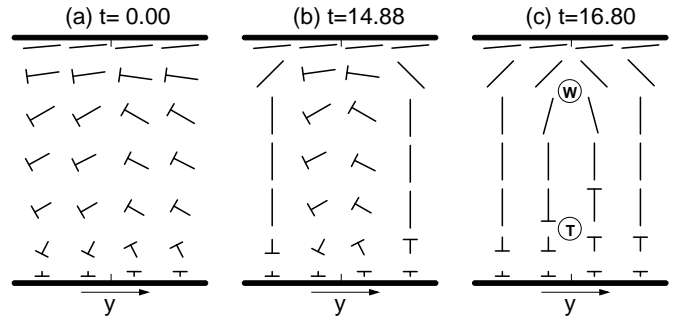


FIG. 7. Nail picture to illustrate the mechanism for the creation of disclination rings in the MD cell. The length of the nail is given by the projection of the director on the drawing plane. Its head symbolizes the part of the director below the drawing plane. a) Undistorted helices, the third and fourth helix have reversed their twisting sense by introducing an additional splay deformation. The helices belong to a path parallel to the y axis indicated in Fig. 6 by an arrow. b) After applying an electric field, the first and fourth helix are destroyed. c) By introducing a twist (T) and a $+1/2$ wedge (W) disclination, the directors in the second and third helix can be aligned along the electric field.

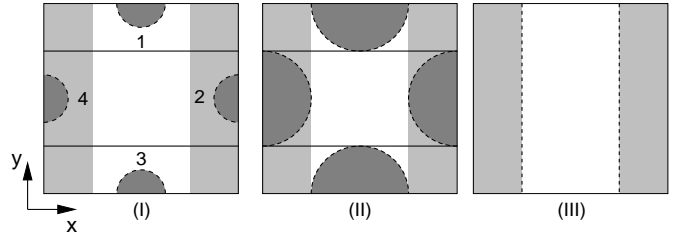


FIG. 8. Mechanism to rotate the disclination lines close to the upper plate by 90° . (I) Disclination rings open up in the regions 1 to 4. (II) They partially annihilate with the existing wedge disclinations. (III) Defect lines of twist character along the y axis result. For a detailed description refer to the text.

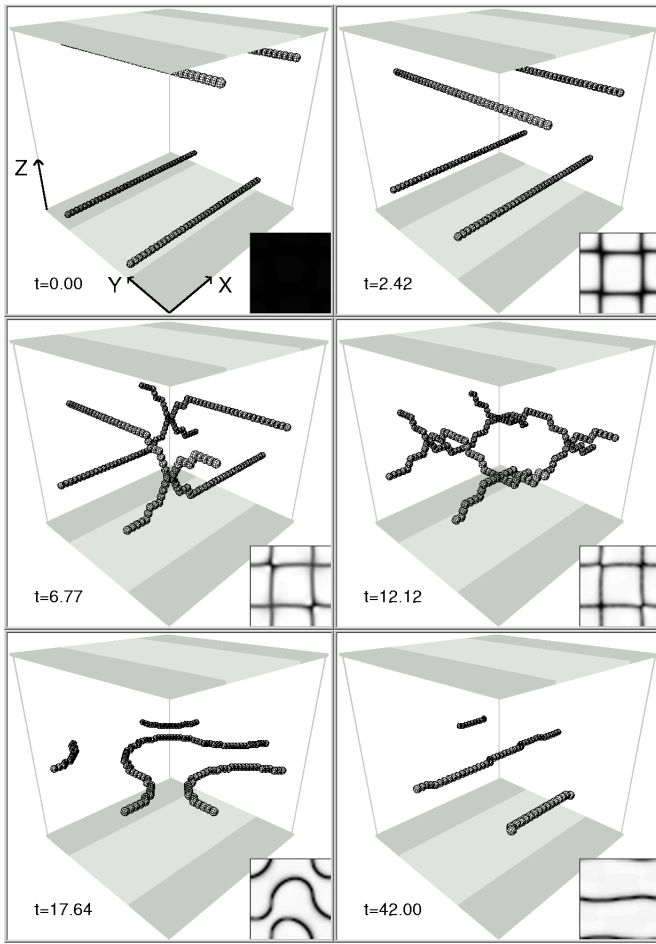


FIG. 9. Snapshots of the partial disappearance of disclinations in the MD cell and its transmission of light (see lower right corner) at various time steps after switching the electric voltage from $U = 4$ V to 0 V. The upper and lower glass plates are divided into anchoring stripes shown in dark and light grey. For a detailed description refer to the text.